AFRL-AFOSR-JP-TR-2022-0073

QUANTUM TECHOLOGIES THAT REJECT THERMAL NOISE FOR IMPROVED SNR IN COHERENT-STATE RANGING AND RELATED APPLICATIONS

Dowling, Jonathan
LOUISIANA STATE UNIVERSITY SYSTEM
3810 W LAKESHORE DR STE 107 SYSTEM B
BATON ROUGE, LA,
US

08/29/2022
Final Technical Report

DISTRIBUTION A: Distribution approved for public release.

Air Force Research Laboratory
Air Force Office of Scientific Research
Asian Office of Aerospace Research and Development
Unit 45002, APO AP 96338-5002

REPORT DOCUMENTATION PAGE

PLEASE DO NOT RETURN YOUR FORM TO THE ABOVE ORGANIZATION.

1. REPORT DATE	2. REPORT TYPE	3. DATES COVERED	
20220829	Final	START DATE 20180705	END DATE 20220704

4. TITLE AND SUBTITLE
QUANTUM TECHOLOGIES THAT REJECT THERMAL NOISE FOR IMPROVED SNR IN COHERENT-STATE RANGING AND RELATED APPLICATIONS

5a. CONTRACT NUMBER	5b. GRANT NUMBER	5c. PROGRAM ELEMENT NUMBER
	FA2386-18-1-4010	61102F
5d. PROJECT NUMBER	**5e. TASK NUMBER**	**5f. WORK UNIT NUMBER**

6. AUTHOR(S)
Jonathan Dowling

7. PERFORMING ORGANIZATION NAME(S) AND ADDRESS(ES)
LOUISIANA STATE UNIVERSITY SYSTEM
3810 W LAKESHORE DR STE 107 SYSTEM B
BATON ROUGE, LA
US

8. PERFORMING ORGANIZATION REPORT NUMBER

9. SPONSORING/MONITORING AGENCY NAME(S) AND ADDRESS(ES)	10. SPONSOR/MONITOR'S ACRONYM(S)	11. SPONSOR/MONITOR'S REPORT NUMBER(S)
AOARD UNIT 45002 APO AP 96338-5002	AFRL/AFOSR IOA	AFRL-AFOSR-JP-TR-2022-0073

12. DISTRIBUTION/AVAILABILITY STATEMENT
A Distribution Unlimited: PB Public Release

13. SUPPLEMENTARY NOTES

14. ABSTRACT
We investigate a few techniques to improve the signal-to-noise-ratio (SNR) of rangefinding, sensing, and other light-detection applications. First technique filters out low photon numbers using photon-number-resolving detectors (PNRDs). This technique has no classical analog and cannot be done with classical detectors.
Then, we use quantum hypothesis testing — a tool of quantum information theory — to show this detection is optimal, for an unknown coherent-state return signal. It is done by deriving the limits of symmetric and asymmetric error probabilities and showing that this detection saturates those quantum limits.
Finally, we show that a coherent state is the optimal probe in the sense that adding squeezing, single-mode and two-mode, does not improve the performance. In particular, quantum illumination does not outperform laser rangefinding when the phase is unusable.
In addition, we checked other techniques; correlation functions and machine learning. Using first-order correlation function, a factor of 2 improvement is obtained, which by repeating N times can be 2N. Unfortunately, Higher order correlation functions don't present any improvement. Moreover, a machine learning code is used, but could not provide the same performance of optimal detection.

15. SUBJECT TERMS

16. SECURITY CLASSIFICATION OF:			17. LIMITATION OF ABSTRACT	18. NUMBER OF PAGES
a. REPORT U	b. ABSTRACT U	c. THIS PAGE U	SAR	25

19a. NAME OF RESPONSIBLE PERSON	19b. PHONE NUMBER *(Include area code)*
MICHAEL RICHARDS	3152277000

Final Report for AOARD Grant 18IOA010

"Quantum Technologies that Reject Thermal Noise in Coherent States"

July 4 2022

Name of Principal Investigators (PI and Co-PIs): Mark M. Wilde (and Lior Cohen)

- E-mail address: mwilde@lsu.edu
- Institution: Louisiana State University
- Mailing Address: 202 Nicholson Hall, Baton Rouge, Louisiana 70803, USA
- Phone: (225) 578-2262
- Fax: (225) 578-5855

Period of Performance: 12/1/2018 – 6/30/2022

Abstract:

We investigate a few techniques to improve the signal-to-noise-ratio (SNR) of rangefinding, sensing, and other light-detection applications. First technique filters out low photon numbers using photon-number-resolving detectors (PNRDs). This technique has no classical analog and cannot be done with classical detectors.

Then, we use quantum hypothesis testing — a tool of quantum information theory — to show this detection is optimal, for an unknown coherent-state return signal. It is done by deriving the limits of symmetric and asymmetric error probabilities and showing that this detection saturates those quantum limits.

Finally, we show that a coherent state is the optimal probe in the sense that adding squeezing, single-mode and two-mode, does not improve the performance. In particular, quantum illumination does not outperform laser rangefinding when the phase is unusable.

DISTRIBUTION A: Distribution approved for public release. Distribution unlimited

In addition, we checked other techniques; correlation functions and machine learning. Using first-order correlation function, a factor of 2 improvement is obtained, which by repeating N times can be 2^N. Unfortunately, Higher order correlation functions don't present any improvement. Moreover, a machine learning code is used, but could not provide the same performance of optimal detection.

General introduction and photon-number thresholding:

Electromagnetic radiation is regularly used for measuring and sensing the physical world. One particular sensing method, namely, laser rangefinding and Light Detection and Ranging (LIDAR) is under continuous development. Increasing the range requires sensitive detectors, and more recently, single-photon detectors (SPDs) [1, 2, 3, 4], and photon-number-resolving detectors (PNRDs) [5, 6] have been used for this purpose.

It is an ongoing question what quantum optics can contribute to applications like LIDAR. It has been proven that loss, such as in rangefinders and LIDARs, eliminates most quantum effects [7, 8], thus, it is ineffective to use quantum states of light for those applications, rather than classical light such as coherent states [9]. However, many proven quantum effects are not a result of using quantum states, but of using quantum detection of these states. For example, Bell-inequality violations are commonly attributed to the use of entangled states [10]. However, all-optical demonstrations have been done with Gaussian states, such as spontaneous parametric down-conversion [11]. It is well known that Bell's inequalities are satisfied when both the state and the detection are Gaussian [12], thus, in all-optical demonstrations, Bell-inequality violations are caused by the non-Gaussian single-photon detection [11]. Having said that, even though rangefinders and LIDARs are operated with coherent states, quantum detection strategies such as parity [9], and photon thresholding (filtering out low photon-numbers) [5] might still give a quantum advantage. In this paper, we rigorously derive the SNR improvement of threshold detection over intensity detection.

One form of laser rangefinding is illustrated in Fig. 1. By sending short pulses of light, and recording their return time, one can measure the range to a target using the speed of light. The rangefinding information can be extended to three-dimensional imaging by adding spatial resolution to the detection. Spatial resolution can be obtained by a gated camera [13], raster scanning [3] or blocking masks [2, 6]. The last method also provides compressed data acquisition, where the number of required measurements is far less than the number of image pixels.

In daylight rangefinding, the classical noise from solar radiation dominates the quantum noise, the latter of which is due to the photon-number fluctuations of the coherent source. Solar radiation is blackbody radiation, and thus, single-mode sunlight has thermal photon-statistics:

$$p_{\rm th}(n) = \frac{\bar{n}_{\rm th}^n}{(\bar{n}_{\rm th}+1)^{n+1}}\,, \tag{1}$$

where $p_{\rm th}(n)$ is the probability to measure n-photons within the coherence time, and $\bar{n}_{\rm th} = (e^{\hbar\omega/k_BT}-1)^{-1}$ is the average photon number, $\hbar$ and k_B are the Dirac and Boltzmann

DISTRIBUTION A: Distribution approved for public release. Distribution unlimited

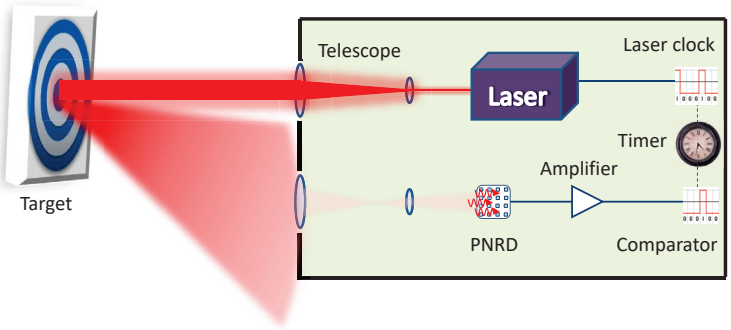

Figure 1: Illustration of the rangefinder system. A laser pulse is sent to a remote target and a small portion is reflected back into the device. After spatial and spectral filtering, the light is detected by a PNRD. Then, the photon number is thresholded by thresholding the voltage height. A one-bit comparator stops the timer when a voltage peak, caused by the detection of a bunch of photons, exceeds the voltage threshold.

constants and ω is the light frequency. The laser is a coherent light source and thus has a Poisson photon distribution:

$$p_{\mathrm{p}}(n) = e^{-\bar{n}_{\mathrm{p}}} \frac{\bar{n}_{\mathrm{p}}^{n}}{n!}\,, \tag{2}$$

where $\bar{n}_{\mathrm{p}}$ is the average photon number. Since the solar flux is continuous, identifying the signal is equivalent to distinguishing a mixture of coherent and thermal light from thermal light alone. The mixture has mixed photon-statistics [14], $p(n) = \sum_{m=0}^{n} p_{\mathrm{p}}(m) p_{\mathrm{th}}(n-m)$ which can be written as

$$p(n) = e^{\frac{\bar{n}_{\mathrm{p}}}{x} - \bar{n}_{\mathrm{p}}} \frac{x^{n}}{n!} \Gamma\left(\frac{\bar{n}_{\mathrm{p}}}{x}, n+1\right), \tag{3}$$

where $x = \bar{n}_{\mathrm{th}}/(\bar{n}_{\mathrm{th}}+1)$, and $\Gamma(y, n+1) = n! e^{-y} \sum_{m=0}^{n} (y^{m}/m!) = \int_{y}^{\infty} t^{n} e^{-t} dt$ is the incomplete gamma function.

Results, Discussion:

Typically, in quantum sensing technologies, it is the shot-noise limit (SNL) that is beaten [15, 16]. While sub-SNL sensitivity can be obtained when the classical noise is negligible, it is a much harder task when the classical noise is dominant [17, 18]. Nevertheless we show that even in this regime, the SNR of quantum detection schemes can still surpass the SNR of classical detection schemes.

Let us compare the classical intensity and our quantum-thresholding detection. Here the signal is regarded as the detection output with the coherent light, and the noise with the thermal light alone. As standard intensity detection is sensitive only to the average number of detected photons, the average photon number of the thermal light alone is the noise and

DISTRIBUTION A: Distribution approved for public release. Distribution unlimited

the sum of the average photon-number of the two light sources is the signal. Thus, the classical SNR is

$$\mathrm{SNR_c} = \frac{\bar{n}_\mathrm{p} + \bar{n}_\mathrm{th}}{\bar{n}_\mathrm{th}} \,. \tag{4}$$

Threshold detection has a binary outcome; it is zero — if the detected photon number is below the threshold photon number, and one — if the detected photon number is above the threshold photon number. The signal of threshold detection is proportional to the probability of successfully exceeding the threshold when coherent light also hits the detector. The noise is proportional to the probability of exceeding the threshold when only thermal light hits the detector. These probabilities are calculated by summing all the photon-number statistics above N, the threshold photon-number.

Thus, the noise is $\nu \sum_{n=N}^{\infty} p_\mathrm{th}(n) = \nu x^N$, and the signal $\nu \sum_{n=N}^{\infty} p(n) = \nu\big[1 - \sum_{n=0}^{N-1} p(n)\big]$, where ν is the number of experimental repetitions. After substituting $p(n)$, reordering the sums and summing over n, we are left with, $\nu\big[1 - \sum_{m=0}^{N-1}\big(1 - x^{N-m}\big)p_\mathrm{p}(m)\big]$. Using the formula of the incomplete gamma function and dividing by the noise, we get that the SNR for threshold detection is:

$$\mathrm{SNR_q} = \frac{1 - \left(\frac{\Gamma(\bar{n}_\mathrm{p}, N)}{(N-1)!} - \frac{\Gamma(\frac{\bar{n}_\mathrm{p}}{x}, N)}{(N-1)!} e^{\frac{\bar{n}_\mathrm{p}}{x} - \bar{n}_\mathrm{p}} x^N\right)}{x^N} \,. \tag{5}$$

Notice that the noise exponentially decays with the threshold number. This decay eventually gives the SNR improvement that we will see in the following.

We wish to get some insights into the expression of Eq. 5. First, we differentiate the SNR with respect to $\bar{n}_\mathrm{p}$,

$$\frac{\partial}{\partial \bar{n}_\mathrm{p}} \mathrm{SNR_q} = \big(\frac{1}{x} - 1\big) \frac{\Gamma(\frac{\bar{n}_\mathrm{p}}{x}, N)}{(N-1)!} e^{\frac{\bar{n}_\mathrm{p}}{x} - \bar{n}_\mathrm{p}} x^N > 0$$

which means that the SNR is a monotonically increasing function of the coherent mean-photon number regardless of the threshold and average thermal photon number. This dependence is expected since increasing the signal intensity should increase the SNR.

Next, we check the threshold dependence on photon number. The difference $[\mathrm{SNR_q}(N+1) - \mathrm{SNR_q}(N)]$ can be written as $[\sum_{n=N}^{\infty} p(n+1) - \sum_{n=N}^{\infty} p(n)x]/x^{N+1}$, where the first summation is transformed as $n \to n+1$. Now the two summations can be regrouped into one, and its argument is $(1-x)p_\mathrm{p}(n+1)$. Thus, the SNR obeys

$$[\mathrm{SNR_q}(N+1) - \mathrm{SNR_q}(N)] = \frac{1-x}{x^{N+1}} \sum_{n=N}^{\infty} p_\mathrm{p}(n+1) > 0 \,, \tag{6}$$

i.e, taking larger photon-number thresholds increases the SNR for any intensity of the coherent and thermal light.

In order to demonstrate the advantage of our quantum scheme, Fig. 2 shows the ratio of the quantum and classical SNR for a fixed average thermal photon number of one. Different threshold photon numbers are plotted with different line widths.

DISTRIBUTION A: Distribution approved for public release. Distribution unlimited

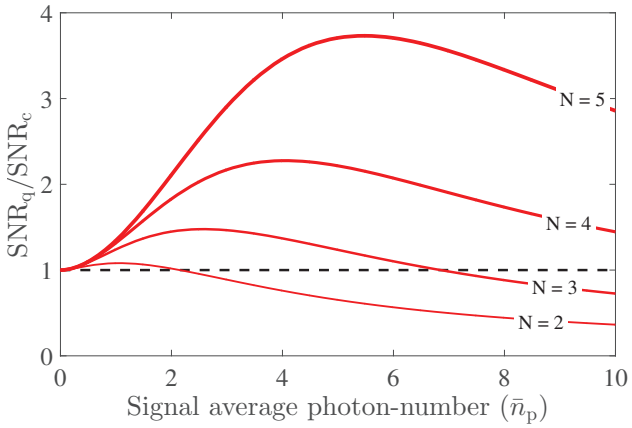

Figure 2: The ratio of the quantum and classical SNR for fixed thermal average photon-number of one. Thresholds of $N = 2, 3, 4, 5$ are plotted where a thicker line corresponds to a higher threshold. The dashed black line at one represents the limit, above which the quantum scheme gets a better SNR.

For many average signal and threshold photon numbers, the ratio of SNR is above one, which means that the quantum SNR exceeds the classical SNR. This improvement is a result of the difference between the signal and noise photon distribution. The thermal distribution is dominant near the low photon numbers, whereas the Poisson distribution is more dominant near the mean photon number. By using threshold detection we exclude low photon numbers where the noise is dominant.

As shown in Eq. 6, the quantum SNR increases when a larger photon number threshold is used. Thus, the ratio of the two SNRs increases with the threshold, since the classical SNR is independent of the threshold. However, taking threshold much larger than the average photon number will cause substantial decrease in the successful threshold detection. Any practical application should choose the threshold photon number in accordance with this trade-off; higher threshold means higher SNR but lower successful threshold detection, lower threshold means higher successful threshold detection but lower SNR. For a practical rangefinder or LIDAR, threshold detection success should be every couple of trials. Thus, in the regime of a few detected signal photons, the best improvement is around four.

In Fig. 2, for every threshold there is an average signal photon number where the improvement is maximal. In Fig. 3a this maximum mean photon number is plotted as a function of the threshold. The improvement is maximal where the threshold is around the mean photon number. This observation can be understood by the fact that the coherent light has a more localized distribution than the thermal light, i.e. the variance of Poisson distribution equals the mean and that of thermal distribution equals the mean square. Thus, if the threshold is well-above the mean photon number of the signal, the detection loses most of the signal, and if it is well below the mean photon number, it is contaminated with noise without gaining signal.

As seen in Fig. 2, the quantum SNR does not always exceed the classical SNR. Figure

DISTRIBUTION A: Distribution approved for public release. Distribution unlimited

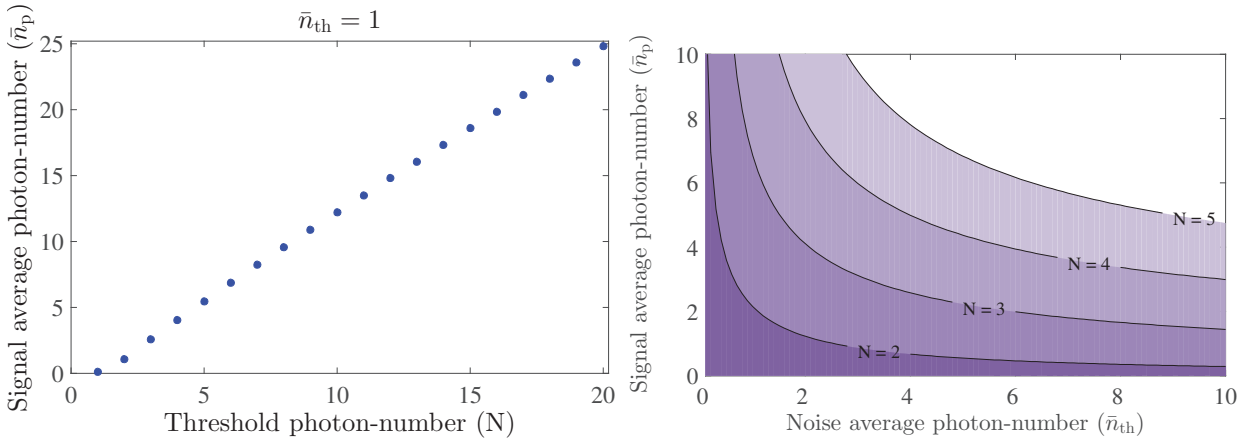

(a) (b)

Figure 3: **(a)** The coherent light (signal) intensity that achieve the best improvement with respect to the classical detection scheme for fixed thermal average photon-number of one. **(b)** Parameter-space representation of the quantum improvement. The line denotes the limit of quantum improvement, where below the line the threshold detection gives higher SNR than the classical detection, for particular threshold number, N. The area under the line increases for larger threshold numbers, showing the improvement achieved by taking larger threshold.

3b is a parameter-space plot, showing the parameters under which quantum detection is superior. Below the line (the darker area) threshold detection presents better SNR. As expected from Eq. 6, the area, where quantum detection outperforms the classical detection, grows as the threshold number is increased. We note that the curved point of each graph holds $N \approx \bar{n}_{\mathrm{th}}$. This fact may help to set the threshold as in most applications the noise intensity is approximately known or can be easily measured.

In the same manner, it seems from the bottom right side of Fig. 3b that threshold detection always gives better results where the noise is high and the signal is low. Thus, in high-noise low-signal regime, threshold detection is definitely preferable.

While Eq. 5 and Fig. 2 show the average results for the quantum SNR and SNR ratio (i.e. infinite ensemble of measurement samplings), most applications may sample the signal only a few times. We simulate multi-target rangefinding to show the improvement with a finite number of samplings. In the simulation, the time is divided to 50 time-bins, where the thermal noise is fixed with $\bar{n}_{\mathrm{th}} = 1$. Each time-bin contains noise photons distributed thermally. Four targets are simulated by adding photons with a Poisson distribution of $0.5\,, 1\,, 3$ and 10 mean photon numbers at times of $10, 20, 30$ and 40, respectively. The simulation runs 100 and 10,000 times, where the former is equivalent to less-than-a-second operation of a typical rangefinder.

The simulation results are shown in Fig. 4. Naturally, the effect of low sampling is larger fluctuations, which can be seen in Fig. 4a, especially for five-photon thresholding where the detection rate is low. The weak target with $\bar{n}_{\mathrm{p}} = 0.5$ is detected well with two-photon

DISTRIBUTION A: Distribution approved for public release. Distribution unlimited

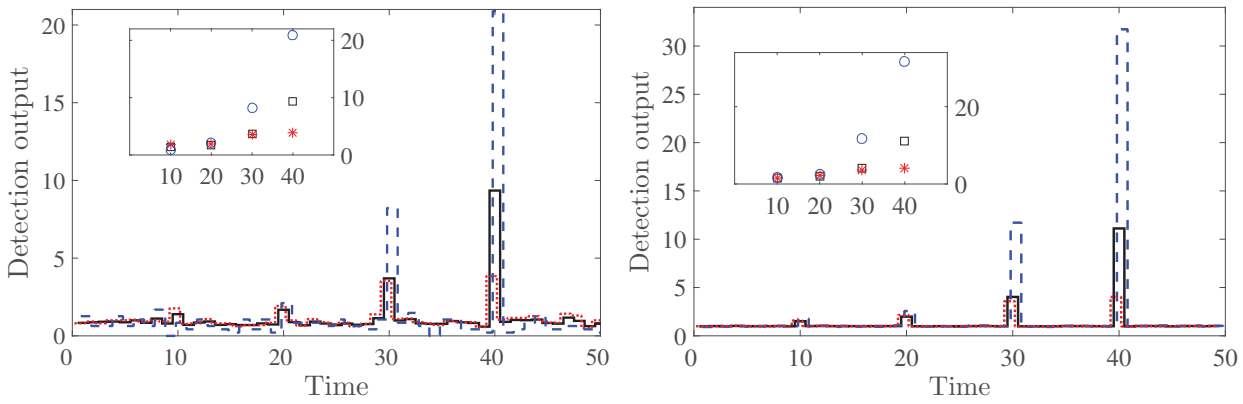

Figure 4: The simulation results comparing intensity detection and thresholding detection for 100 **(a)** and 10,000 **(b)** repetitions. The intensity detection is plotted with solid black line, two-photon thresholding with red dotted line, and five-photon thresholding with blue dashed line. The three graphs are slightly shifted, for visual purposes. The signal height is normalized such that the noise average is one. The inset shows the same comparison only for the time bins with the coherent photons. The intensity detection is plotted with black boxes, two-photon thresholding with red asterisks, and five-photon thresholding with blue circles.

thresholding but not detected at all with five-photon thresholding. This effect is again due to the detection rate. When the number of simulation repetitions is increased, the ratio of the SNR approaches the values of Fig. 2. For the target with $\bar{n}_{\mathrm{p}} = 10$, the output of five-photon thresholding is 31.7 and of intensity is 11.1. As the noise is normalized to one, the ratio of the SNR is just $\frac{31.7}{11.1} = 2.86$ which is exactly the result of Fig. 2. For the weak target with $\bar{n}_{\mathrm{p}} = 0.5$, the output of two-photon thresholding is 1.58, of five-photon thresholding is 1.77 and of intensity is 1.51, which gives SNR ratio of 1.04 and 1.17 where 1.05 and 1.10 are deduced from Fig. 2.

We propose to implement the threshold detector with PNRD. There may be other implementation methods, such as N-photon-ionization processes. Additionally, other detection protocols using PNRDs may give higher gain of the localized photon distribution, and thus, better SNR improvement. Examples include exact photon-number detection (i.e. projecting on a specific Fock state) [19] and a range of photon-number detection. These protocols require knowledge about the signal intensity and are suited to applications with known signal intensity. Threshold detection does not require knowledge about the signal intensity, and thus is suited to applications like rangefinding and LIDAR, where the signal intensity is a priory unknown.

After we published the thresholded quantum-LIDAR paper, we had a few discussions regarding the paper [20]. One question, raised from those discussions, was how the SNR should be defined. One way to define the SNR is to compare the detection output with and

DISTRIBUTION A: Distribution approved for public release. Distribution unlimited

without the signal photons. In this case, the classical SNR is [21, 22]:

$$\mathrm{SBR_c} = \frac{\bar{n}_\mathrm{p} + \bar{n}_\mathrm{th}}{\bar{n}_\mathrm{th}} \,. \tag{7}$$

For clarity, we rename this SNR as signal to background ratio (SBR). Alternatively, the SNR can be defined as the detection output difference (with and without signal photons) over the total noise. In this case the classical SNR is [23]:

$$\mathrm{SNR_c} = \frac{\bar{n}_\mathrm{p} - \bar{n}_\mathrm{th}}{\sqrt{\Delta^2(n_\mathrm{p} + n_\mathrm{th}) + \Delta^2 n_\mathrm{th}}} = \frac{\bar{n}_\mathrm{p} - \bar{n}_\mathrm{th}}{\sqrt{\bar{n}_\mathrm{p} + 2\bar{n}_\mathrm{th}(1 + \bar{n}_\mathrm{th})}} \,. \tag{8}$$

Threshold detection has a binary outcome; it outputs zero if the detected photon number is below the threshold photon number, and it outputs one if the detected photon number is above the threshold photon number. Thus, the detector output without the signal photons is $\gamma_\mathrm{th} = \sum_{n=N}^{\infty} p_\mathrm{th}(n) = x^N$, and with them it is $\gamma_\mathrm{p} = \sum_{n=N}^{\infty} p(n) = \left[1 - \sum_{n=0}^{N-1} p(n)\right]$. After substituting $p(n)$, reordering the sums and summing over n, we are left with, $\gamma_\mathrm{p} = \left[1 - \sum_{m=0}^{N-1} \left(1 - x^{N-m}\right) p_\mathrm{p}(m)\right]$. Using the formula of the incomplete gamma function and dividing by the noise, we get that $\gamma_\mathrm{p} = 1 - \left(\frac{\Gamma(\bar{n}_\mathrm{p}, N)}{(N-1)!} - \frac{\Gamma(\frac{\bar{n}_\mathrm{p}}{x}, N)}{(N-1)!} e^{\frac{\bar{n}_\mathrm{p}}{x} - \bar{n}_\mathrm{p}} x^N\right)$. Therefore, the SBR and SNR for threshold detection are as follows:

$$\mathrm{SBR_q} = \frac{\gamma_\mathrm{p}}{\gamma_\mathrm{th}} \,, \tag{9}$$

$$\mathrm{SNR_q} = \frac{\gamma_\mathrm{p} - \gamma_\mathrm{th}}{\sqrt{\gamma_\mathrm{p}(1 - \gamma_\mathrm{p}) + \gamma_\mathrm{th}(1 - \gamma_\mathrm{th})}} \,. \tag{10}$$

As seen in Figure 5, both measures show quantum enhancement; i.e., the quantum SNR (SBR) is greater than the classical SNR (SBR). SBR and SNR are two measures for evaluating the performance of a LIDAR system, but not the only ones [21, 22, 23]. It is interesting to consider different measures like the error probability in further research.

Introduction to quantum hypothesis testing:

One of the main goals of quantum information theory [24, 25, 26, 27] is to identify the ultimate limits of information-processing tasks. One such basic task is the discrimination of two quantum states, and this problem is known as quantum hypothesis testing [28, 29, 30].

There are various ways of measuring the performance of hypothesis testing, and two prominent methods are known as symmetric and asymmetric hypothesis testing. In the former, there is an assumed prior probability distribution on the two states, and the goal is to minimize the average error probability of misidentifying the states. In the latter, no prior probability distribution is assumed, and the goal is to minimize the probability of a missed detection error (Type II), subject to a constraint on the false alarm error probability (Type I).

A sensing task, which measures an unknown physical quantity of a system, is usually accomplished by detecting a probe state that interacts with the system [17]. The interaction

DISTRIBUTION A: Distribution approved for public release. Distribution unlimited

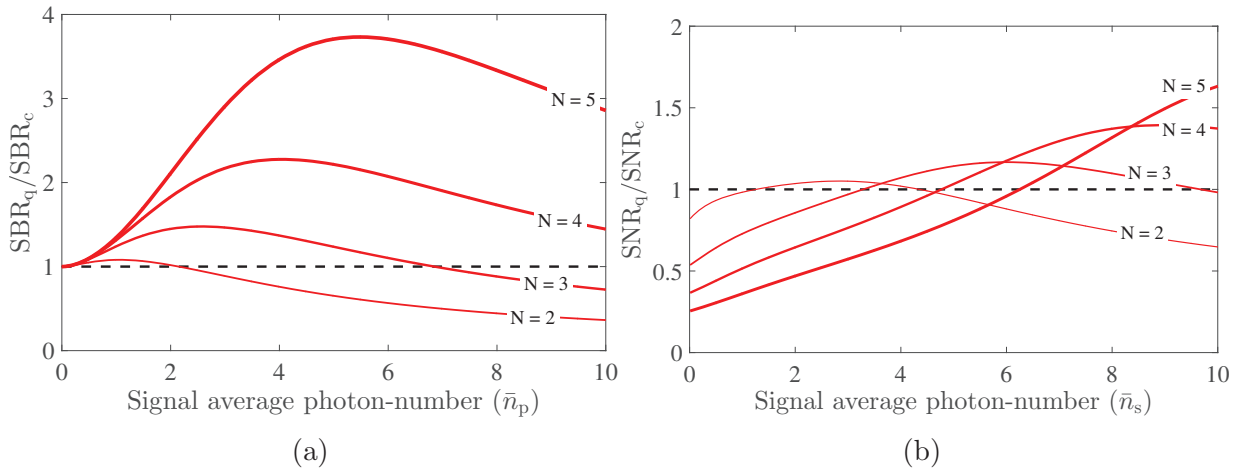

(a) (b)

Figure 5: The ratio of the quantum and classical SBR (a) and SNR (b) for fixed thermal average photon-number of one. Thresholds of $N = 2, 3, 4, 5$ are plotted where a thicker line corresponds to a higher threshold. The dashed black line at one represents the limit, above which the quantum scheme gets a better SBR/SNR.

results in a change of the probe state, and this change depends on the physical quantity of interest. Then identifying the probe state extracts the quantity's value [31]. Thus, there is an intimate connection between quantum information processing and quantum sensing.

In particular, for the well-known setting of range finding and LIDAR, a short laser pulse is transmitted in a direction in which a target is suspected to be present (see Figure 6). If the target is present, the return state is a mixture of the original laser light and the background light, which is thermal. If the target is absent, then the return state is just thermal background light. Thus, discriminating between a thermal state and a mixture of a thermal and coherent state is equivalent to sensing the presence or absence of the target (known as target detection).

Target detection has been shown to be one of the tasks that can be improved by using quantum probes [32, 21]. This is typically conducted, as mentioned, by differentiating between two and only two states: one representing the presence of a target and the other the absence. However, a hidden assumption is present in this commonly employed model: if the target is present, the return state is assumed to be known; in particular, its intensity and phase are assumed to be known. While the optimal detection – the detection that saturates the quantum limit – might be known [33] and implementable in principle, it uses all the information available about the two states. Thus, for ranging applications, in which the intensity and phase of the return state are often unknown, different limits should be found, and another detection scheme should be devised. This motivates the results reported in here. The results of quantum target detection are still valuable for a fixed range with a known phase, i.e., imaging.

Here, we tackle the problem of detecting an unknown return state, by proceeding in two steps. As a first step, we lift the assumption of known intensity but leave the phase fixed

DISTRIBUTION A: Distribution approved for public release. Distribution unlimited

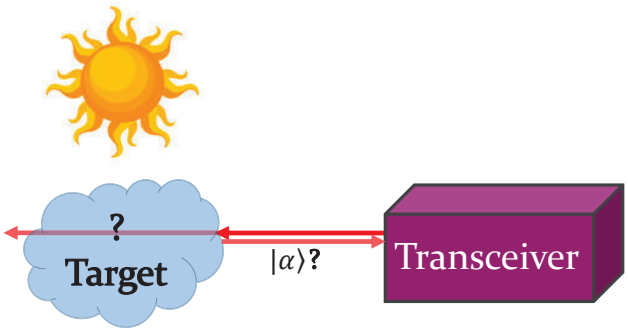

Figure 6: Illustration of a typical ranging setup. A short laser pulse is sent to a potential target. If the target is present, an unknown coherent state is received together with the background. If the target is absent, only the background thermal state is detected.

and known. The physical scenario corresponding to this step is one in which the range is fixed but the attenuation is unknown. As a second step, we lift the assumption of a known phase, which corresponds to the general scenario of ranging applications. More precisely, we calculate the bounds for the symmetric and asymmetric single-shot error probabilities, and we then devise a single detection scheme and measurement to minimize the error probabilities over all possible return states. To verify the theory presented here, we have also performed numerical simulations.

Setup and background—In range finding and LIDAR, a short pulse of a laser is sent towards a potential target with an unknown range. The fragment of the laser light is detected by a receiver. In the absence of the laser light, a thermal state is received (corresponding to the thermal background), denoted by the state ρ_{th} and defined as

$$\rho_{\text{th}} \coloneqq \frac{1}{1+\bar{n}_{\text{th}}} \sum_{n=0}^{\infty} \left(\frac{\bar{n}_{\text{th}}}{1+\bar{n}_{\text{th}}} \right)^n |n\rangle\langle n| \,, \tag{11}$$

where $\bar{n}_{\text{th}}$ is the average photon number, and $|n\rangle$ is the n-photon number state. Henceforth, the Fock basis is used to represent the states. (See Ref. [34] for background on quantum optics.) In the presence of the target, the received state is a displaced thermal state ρ_{s}, defined as

$$\rho_{\text{s}} \coloneqq \hat{D}(\alpha)\rho_{\text{th}}\hat{D}(\alpha)^\dagger \,, \tag{12}$$

where $\hat{D}(\alpha) = e^{i(\alpha\hat{a}^\dagger - \alpha^*\hat{a})}$ is the displacement operator and $\alpha = e^{i\phi}|\alpha|$ is the parameter of the unknown coherent state reflected from the target. The amplitude $|\alpha|$ is determined by the overall attenuation of the round trip to the target and back, and the parameter ϕ in $e^{i\phi}$ is the overall accumulated phase. In particular, both parameters depend on the range to the target. Notice that we assume here that the laser light and the background light interfere and the received light is always a single mode. The displaced thermal state ρ_{s} is represented in the number-state basis as follows:

$$\langle n|\rho_{\text{s}}|m\rangle = \frac{1}{1+\bar{n}_{\text{th}}} \sum_{k=0}^{\infty} \left(\frac{\bar{n}_{\text{th}}}{1+\bar{n}_{\text{th}}} \right)^k \langle n|\hat{D}(\alpha)|k\rangle\langle m|\hat{D}(\alpha)|k\rangle^* \,, \tag{13}$$

DISTRIBUTION A: Distribution approved for public release. Distribution unlimited

and the number-state representation $\langle n|\hat{D}(\alpha)|m\rangle$ of the displacement operator $\hat{D}(\alpha)$ is as follows [35]:

$$\langle n|\hat{D}(\alpha)|m\rangle = \begin{cases} e^{\frac{-|\alpha|^2}{2}}\sqrt{\frac{m!}{n!}}e^{i\phi(m-n)}(-|\alpha|)^{n-m}L_m^{(n-m)}(|\alpha|^2) & n \geq m \\ e^{\frac{-|\alpha|^2}{2}}\sqrt{\frac{n!}{m!}}e^{i\phi(m-n)}|\alpha|^{m-n}L_n^{(m-n)}(|\alpha|^2) & m \geq n \end{cases}, \tag{14}$$

where $L_n^{(k)}(x)$ is a generalized Laguerre polynomial.

Symmetric error setting:

For a single-shot experiment, the optimal symmetric error probability is given by the Helstrom bound [36, 28]:

$$p_{\text{err}}^H = \frac{1}{2}\left(1 - \frac{1}{2}\|\rho_{\text{s}} - \rho_{\text{th}}\|_1\right), \tag{15}$$

where $\rho_{\text{s/th}}$ are the two states under question and $\|\cdot\|_1$ is the trace norm. Related to this, the limit of a specific measurement channel $\mathcal{M}$ is given by

$$p_{\text{err}}^H(\mathcal{M}) = \frac{1}{2}\left(1 - \frac{1}{2}\|\mathcal{M}(\rho_{\text{s}}) - \mathcal{M}(\rho_{\text{th}})\|_1\right), \tag{16}$$

where $\mathcal{M}(\omega)$ denotes the probability distribution resulting from the measurement acting on the state ω and $\|\cdot\|_1$ in this case denotes the ℓ_1 distance of the two probability distributions.

The Helstrom bound as a function of the return intensity is plotted as the dotted blue curve in Figure 7a. Reaching the Helstrom bound is accomplished by optimizing over all possible measurements. In this work, we limit the measurement setup to displacement operations followed by photon-number detection, known as the generalized Kennedy receiver [37, 38]. This measurement scheme is experimentally realizable but does not generally achieve the Helstrom bound. It has been used for the related problem of discriminating a thermal state from a coherent state and demonstrated error probabilities close to the Helstrom bound for that problem [39]. Furthermore, photon-number detection has been demonstrated in LIDARs [6]. Optimizing over displacements, the limit of this measurement setup is calculated by Eq. (16) and is depicted as the green solid curve in Figure 7a. We note that the displacement is optimized for $N_{\text{s}} = 1$ and has been kept fixed for all intensities, because we have assumed that the intensity is unknown to the receiver.

To validate the theory outlined above, we have performed numerical simulations that replicate the results of a ranging experiment. A photon number n is randomly chosen, based on the probability distributions that result when the target is either absent or present. For photon number detection, the optimal decision rule is the well-known Neyman–Pearson test [40]:

$$p_{\text{s}}(n) - p_{\text{th}}(n) \geq 0, \tag{17}$$

where $p_{\text{s}}(n) \coloneqq \langle n|\hat{D}(\beta)\rho_{\text{s}}\hat{D}^\dagger(\beta)|n\rangle$ is the probability of measuring n photons after optimal displacement (β) with a target and $p_{\text{th}}(n) \coloneqq \langle n|\hat{D}(\beta)\rho_{\text{th}}\hat{D}^\dagger(\beta)|n\rangle$ after optimal displacement

DISTRIBUTION A: Distribution approved for public release. Distribution unlimited

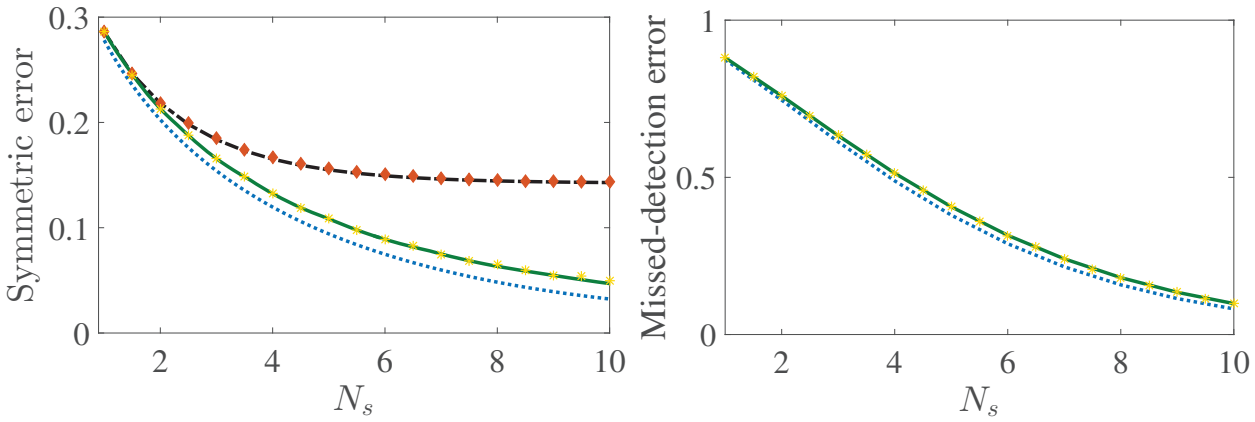

(a) (b)

Figure 7: Symmetric (a) and asymmetric (b) error probabilities as a function of the intensity of the return signal with a known phase. The quantum limit is shown by a blue dotted curve. The limit of photon-number detection after optimal displacement is presented with a green solid curve. The simulated data are presented with yellow stars. For the symmetric error setting, simulated data without changing the measurement are presented with orange diamonds. These data fit to the theoretical prediction (black short-dashed curve). The average photon number of the thermal source is set to 1. For the asymmetric error, the false-alarm error probability threshold is set to 0.01. See text for more details.

without a target. If the inequality in Eq. (17) is satisfied, the receiver concludes that the target is present, and if the inequality is violated, the receiver concludes that a target is not present. In our numerical simulations, we have repeated the detections a large number of times and counted the number of times that the receiver guesses incorrectly, leading to the average error probability presented by yellow stars in Figure 7a.

We arrive at one immediate conclusion from the simulations: to reach the measurement limit, the photon number distribution is used. However, it is impossible to do this in a single shot if the intensity is unknown. A possible solution is to fix $p_{\rm s}(n)$ in the decision rule to be the photon number distribution for $N_{\rm s} = 1$. The new theoretical prediction and the simulation results for that are also plotted in Figure 7a, as a dashed black line and orange diamonds.

Asymmetric error setting:

Next, we consider the setting of asymmetric error probability (see, e.g., [24] for the general case and [41] in the context of bosonic Gaussian states). In this setting, the false-alarm error probability is constrained to be below $\varepsilon \in (0, 1)$, and the missed-detection error probability is minimized subject to this constraint. The quantum-limited error probability is then given

DISTRIBUTION A: Distribution approved for public release. Distribution unlimited

by

$$\beta(\varepsilon) \coloneqq \min_{\hat{\Lambda}} \{ \mathrm{Tr}(\hat{\Lambda}\rho_{\mathrm{s}}) \,|\, 0 \leq \hat{\Lambda} \leq I,\, \mathrm{Tr}(\hat{\Lambda}\rho_{\mathrm{th}}) \geq 1-\varepsilon \}\,, \tag{18}$$

where the minimization is performed over every measurement operator $\hat{\Lambda}$ satisfying $\mathrm{Tr}(\hat{\Lambda}\rho_{\mathrm{th}}) \geq 1-\varepsilon$. This optimization can be performed using semi-definite programming [42], which allows for calculating $\beta(\varepsilon)$ numerically.

The ultimate limit is displayed by the dotted blue curve in Figure 7b. This limit can be modified for a specific measurement scheme $\mathcal{M}$ by replacing the states ρ_{s} and ρ_{th} with $\mathcal{M}(\rho_{\mathrm{s}})$ and $\mathcal{M}(\rho_{\mathrm{th}})$, respectively. Taking the measurement $\mathcal{M}$ to be photon-number detection after optimal displacement, the modified limit is depicted with a green solid curve in Figure 7b.

In the case that we first perform a displacement and photon-number detection on the states involved, the optimal operator $\hat{\Lambda}$ has a simplified form, diagonal in the photon-number basis, and becomes equivalent to a stochastic decision rule. It takes the following form

$$\hat{\Omega} = \sum_{n=0}^{\infty} \Omega(n) |n\rangle\langle n|\,, \tag{19}$$

where $\Omega(n) \in [0,1]$ for all n, so that each $\Omega(n)$ corresponds to the probability of deciding that the target is present.

Using the same simulation procedure described above, we have generated simulated data for the setting involving asymmetric error probability. For a drawn photon number n, the receiver decides that the target is present with probability $\Omega(n)$ and that the target is absent with probability $1-\Omega(n)$. The probability $\Omega(n)$ is found by the minimization procedure given in Eq. (18) after applying the optimal displacement and photon-number detection (see also Figure 10). The single-shot error probability is obtained by averaging the simulation results and plotted as yellow stars in Figure 7b. In this setting, unlike that for symmetric error probability, the optimal measurement is set only by the thermal state through the condition $\mathrm{Tr}(\hat{\Lambda}\rho_{\mathrm{th}}) \geq 1-\varepsilon$. Thus, the same measurement is used for every signal intensity, and it is not affected by the unknown signal intensity.

Unknown phase:

Up until this point, we have considered a return signal state having a known and fixed phase. The phase was used when optimizing the displacement and when calculating the photon number distribution. In a typical single-shot ranging experiment, however, the phase is not known; thus, to calculate the average error probability for an unknown phase, one should integrate over all phases. When doing that, the results of the average errors are much worse than those in the scenario involving with known and fixed phase. This is a result of using a measurement that is phase sensitive when the phase is unknown. Moreover, in a single-shot experiment, one cannot determine if the return state has a fixed phase or an unstable phase. Thus, it can be assumed to be the latter. In this case, the signal state is

$$\rho_{\mathrm{s}}' = \frac{1}{2\pi} \int_0^{2\pi} d\phi\ \rho_{\mathrm{s}}(\phi), \tag{20}$$

DISTRIBUTION A: Distribution approved for public release. Distribution unlimited

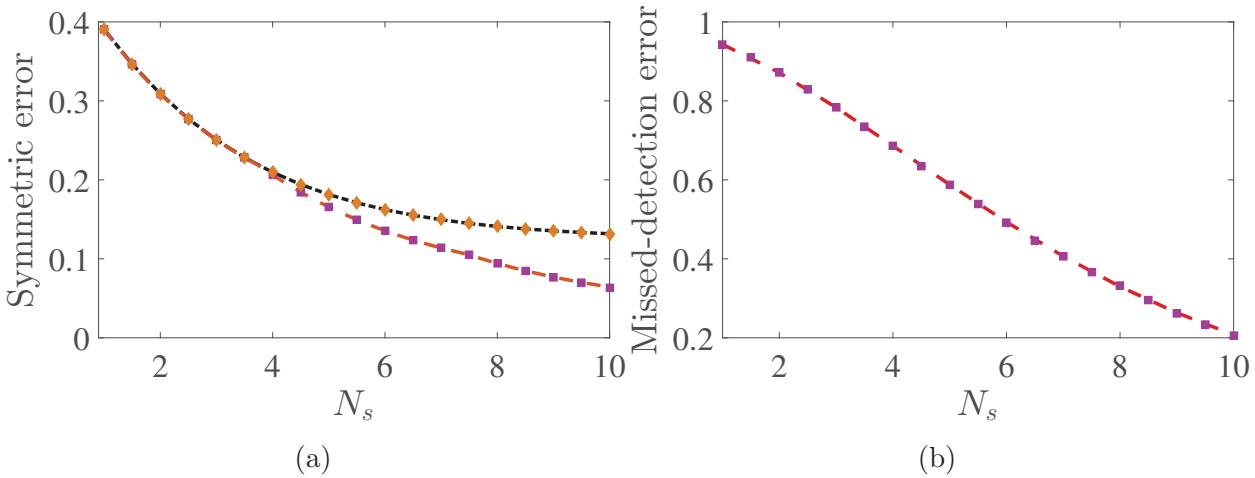

Figure 8: (a) Symmetric and (b) asymmetric error probabilities as a function of the intensity of the return signal with an unstable phase. The quantum limit is depicted as a red dashed curve. The simulated data are presented with purple boxes. For the symmetric error probability, simulated data without changing the measurement are depicted as orange diamonds. These data fit the theoretical prediction, which is depicted as a black short-dashed curve. The average photon number of the thermal source is set to 1. For the asymmetric error probability, the false-alarm error probability is set to 0.01. See the main text for more details.

where here, for clarity, we have written $\rho_{\rm s}(\phi) := \hat{D}(\alpha)\rho_{\rm th}\hat{D}(\alpha)^\dagger$ to indicate the explicit dependence of the state of Eq. (12) on the phase ϕ, where $\alpha = |\alpha|e^{i\phi}$. Since

$$\langle n|\hat{D}(\alpha)|k\rangle\langle m|\hat{D}(\alpha)|k\rangle^* \propto e^{i\phi(m-n)}, \tag{21}$$

then

$$\int_0^{2\pi} \langle n|\hat{D}(\alpha)|k\rangle\langle m|\hat{D}(\alpha)|k\rangle^* d\phi \propto \delta_{n,m}. \tag{22}$$

That is, this expression is equal to zero if $n \neq m$. Plugging this observation into Eq. (13), we find that the matrix elements of the dephased state $\rho'_{\rm s}$ are given by [43]

$$\langle n|\rho'_{\rm s}|m\rangle = \frac{\bar{n}_{\rm th}^n}{(1+\bar{n}_{\rm th})^{n+1}} \exp\left(-\frac{|\alpha|^2}{1+\bar{n}_{\rm th}}\right) L_n\left(-\frac{|\alpha|^2}{(1+\bar{n}_{\rm th})\bar{n}_{\rm th}}\right) \delta_{n,m}\,. \tag{23}$$

Therefore, in the case of an unstable phase for the return signal, the state has no phase information and a phase-insensitive measurement is optimal.

We repeat the same analysis for the unstable phase state. The Helstrom bound and the missed-detection error probability bound are plotted with red dashed curves in Figures 8a and 8b, respectively. The simulations are reproduced with one difference; there is no displacement that impacts the photon statistics. The average error probabilities from the simulation are plotted as purple boxes in Figures 8a and 8b. Similar to the known phase case, the optimal

DISTRIBUTION A: Distribution approved for public release. Distribution unlimited

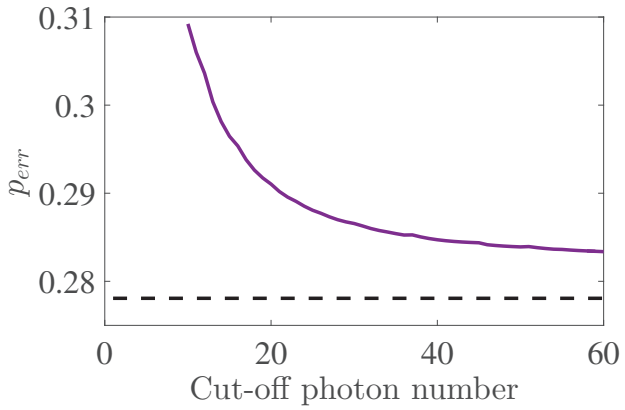

Figure 9: Symmetric error probability as a function of cutoff photon number. The black dashed line is the Helstrom bound. Using higher photon-number resolution enables to intensify the displacement and to get closer to the Helstrom bound.

symmetric error probability uses the information about the photon statistics of the return signal state. If this use is prevented, the simulation results imply that there is a larger error probability. This is in agreement with the theoretical prediction.

Discussion:

For the known phase case, we found that applying an optimal displacement followed by photon-number detection leads to an error probability that is near the quantum limit. This detection strategy is phase sensitive and works well when the phase is fixed and known, but less well for the unstable phase case. Regardless, when we apply this strategy to the latter case, the error probability is higher than when applying a phase-insensitive measurement.

The optimal displacement is highly sensitive to the chosen cutoff photon number. Increasing the cutoff number increases the optimal displacement parameter and decreases the error probability. The error probability as a function of the cutoff number is depicted in Figure 9. We speculate that in the limit of infinite displacement (and infinite photon-number resolution), this measurement scheme saturates the quantum bound. In the other figures and simulations, we have employed a cutoff of 30 photons.

For the setting involving symmetric error probability, the classical decision rule after performing a photon number measurement with an outcome of n photons, preceded by or not preceded by displacement, is conducted by checking the sign of $p_{\mathrm{s}}(n) - p_{\mathrm{th}}(n)$. It can be shown that the two probabilities under question intersect only in one point. This means $p_{\mathrm{th}}(n)$ is larger up to some photon number — the threshold photon number — and smaller after it. Thus, no target is presumably detected if a photon number less than the threshold is measured, and the target is presumably detected if a larger photon number is measured. Thus, we have found that the near-optimal detection is photon-number thresholding [20] after displacement. For the case of unstable phase, photon number thresholding is optimal.

In general, for ranging applications, the setting with asymmetric error probability is more

DISTRIBUTION A: Distribution approved for public release. Distribution unlimited

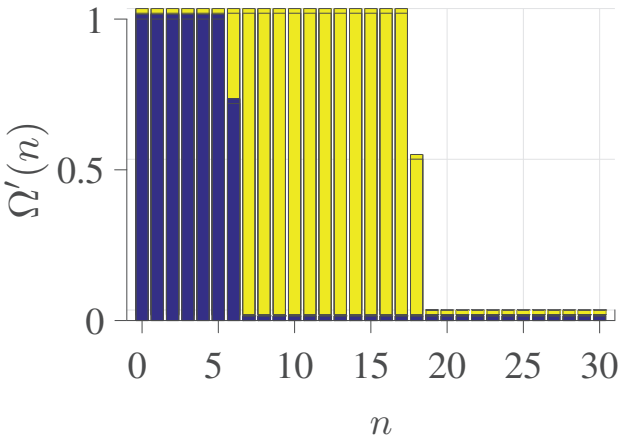

Figure 10: Acceptance probabilities as a function of measured photon number. The back yellow bars are the acceptance probabilities for the simulated data of Figure 7a, and the front blue bars are the acceptance probabilities for the simulated data of Figure 8a. See text for more details.

applicable than the symmetric setting. This is because one is typically willing to tolerate false-detection errors at a fixed rate and then the goal is to minimize the rate of missed-detection errors. Thus, saturating the quantum limit for this error has higher importance. Fortunately, for the setting of asymmetric error probability, our results follow the quantum limit for the known phase case and saturate it for the unknown phase case.

For the setting with asymmetric error probability, the decision rule upon measuring n photons is random, i.e., the stochastic decision rule $\Omega(n)$, found in Eq. (19). The probabilities for this stochastic decision rule are displayed in Figure 10, for the measurements used in Figures 7b and 8b. Those measurements are very close to threshold detection, since the acceptance probabilities are equal to zero for low photon number and equal to one for high photon number (which also makes the decision deterministic). The only difference is that the value for the intermediate photon number is not an integer. This causes a non-deterministic choice, unlike threshold detection. This measurement can be thought of as a generalization of a non-integer photon-number threshold detection — it passes for every detected photon number larger than the threshold photon number, it fails for every photon number lower than the threshold, and passes randomly if the detected photon number equals the threshold. This generalized threshold detection can be realized in the lab by setting the threshold voltage in the middle of the Gaussian packet of the threshold photon number, instead of being in between Gaussian packets of different photon numbers. Thus, when the detected photon number equals the threshold, a target is announced randomly based on the electronic noise, which serves as a random generator.

While threshold detection has been suggested for ranging applications [20], it has not been proven to be optimal. Here, not only do we demonstrate that it is optimal (at least for the asymmetric setting), but we also present the protocol that sets the optimal threshold.

A practical experimental setup suffers from imperfections. The presented protocol can

DISTRIBUTION A: Distribution approved for public release. Distribution unlimited

be easily modified to fit modeled imperfections. Usually, optical loss is the most significant effect. However, here it does not affect our results, given that a displaced thermal state remains such after loss. All the above discussion is then conducted on the measured state, i.e., after loss. Other imperfections will change the measured photon statistics [44]. Since this change is modeled and known, the rest of the detection protocol stays the same but then is conducted with the modified statistics.

List of Publications and any Significant Collaborations that resulted from your AOARD supported project:

- L. Cohen and M. M. Wilde. "Toward Optimal Quantum Ranging: Hypothesis Testing for an Unknown Return Signal," *Phys. Rev. Applied* **17**, 044053 (2022).
- L. Cohen and M. M. Wilde. "Optimal Quantum Ranging—Hypothesis Testing for an Unknown Return Signal," In Quantum Information and Measurement, pp. M2B-4. Optical Society of America, (2021).
- L. Cohen, A. J. Brady, Z. Huang, H. Liu, D. Qu, J. P. Dowling, and M. Han. "Simulation of Loop Quantum Gravity–A Scalable Linear-Optical Approach," *Phys. Rev. Lett.* **126**, 020501 (2021).
- L. Cohen, A. J. Brady, Z. Huang, H. Liu, D. Qu, J. P. Dowling, and M. Han. "Simulation of Loop Quantum Gravity–A Scalable Linear-Optical Approach," In Frontiers in Optics, pp. FTu6D-4. Optical Society of America, (2020).
- L. Cohen, E. S. Matekole, Y. Sher, D. Istrati, H. S. Eisenberg, and J. P. Dowling." Thresholded Quantum LIDAR: Exploiting Photon-Number-Resolving Detection," *Phys. Rev. Lett.* **123**, 203601 (2019).
- L. Cohen, E. S. Matekole, Y. Sher, D. Istrati, H. S. Eisenberg, and J. P. Dowling." Thresholded Quantum LIDAR: Exploiting Photon-Number-Resolving Detection," In Conference on Coherence and Quantum Optics, pp. M5A-14. Optical Society of America (2019).
- L. Cohen, E. S. Matekole, Y. Sher, D. Istrati, H. S. Eisenberg, and J. P. Dowling." Filtering Coherent Signal from Thermal Noise by Photon-Number Thresholding," In Frontiers in Optics, pp. JTu4A-44. Optical Society of America (2019).

References

[1] R. E. Warburton, A. McCarthy, A. M. Wallace, S. Hernandez-Marin, R. H. Hadfield, S. W. Nam, and G. S. Buller, "Subcentimeter depth resolution using a single-photon counting time-of-flight laser ranging system at 1550 nm wavelength," *Optics letters*, vol. 32, no. 15, pp. 2266–2268, 2007.

DISTRIBUTION A: Distribution approved for public release. Distribution unlimited

[2] G. A. Howland, D. J. Lum, M. R. Ware, and J. C. Howell, "Photon counting compressive depth mapping," *Optics express*, vol. 21, no. 20, pp. 23822–23837, 2013.

[3] A. M. Pawlikowska, A. Halimi, R. A. Lamb, and G. S. Buller, "Single-photon three-dimensional imaging at up to 10 kilometers range," *Optics express*, vol. 25, no. 10, pp. 11919–11931, 2017.

[4] Z.-P. Li, X. Huang, Y. Cao, B. Wang, Y.-H. Li, W. Jin, C. Yu, J. Zhang, Q. Zhang, C.-Z. Peng, *et al.*, "Single-photon computational 3d imaging at 45 km," *arXiv preprint arXiv:1904.10341*, 2019.

[5] Z. Bao, Y. Liang, Z. Wang, Z. Li, E. Wu, G. Wu, and H. Zeng, "Laser ranging at few-photon level by photon-number-resolving detection," *Applied optics*, vol. 53, no. 18, pp. 3908–3912, 2014.

[6] Y. Sher, L. Cohen, D. Istrati, and H. S. Eisenberg, "Low intensity lidar using compressed sensing and a photon number resolving detector," in *Emerging Digital Micromirror Device Based Systems and Applications X*, vol. 10546, p. 105460J, International Society for Optics and Photonics, 2018.

[7] U. Dorner, R. Demkowicz-Dobrzanski, B. Smith, J. Lundeen, W. Wasilewski, K. Banaszek, and I. Walmsley, "Optimal quantum phase estimation," *Physical review letters*, vol. 102, no. 4, p. 040403, 2009.

[8] T.-W. Lee, S. D. Huver, H. Lee, L. Kaplan, S. B. McCracken, C. Min, D. B. Uskov, C. F. Wildfeuer, G. Veronis, and J. P. Dowling, "Optimization of quantum interferometric metrological sensors in the presence of photon loss," *Physical Review A*, vol. 80, no. 6, p. 063803, 2009.

[9] K. Jiang, H. Lee, C. C. Gerry, and J. P. Dowling, "Super-resolving quantum radar: Coherent-state sources with homodyne detection suffice to beat the diffraction limit," *Journal of Applied Physics*, vol. 114, no. 19, p. 193102, 2013.

[10] X.-F. Qian, B. Little, J. C. Howell, and J. Eberly, "Shifting the quantum-classical boundary: theory and experiment for statistically classical optical fields," *Optica*, vol. 2, no. 7, pp. 611–615, 2015.

[11] M. Giustina, A. Mech, S. Ramelow, B. Wittmann, J. Kofler, J. Beyer, A. Lita, B. Calkins, T. Gerrits, S. W. Nam, *et al.*, "Bell violation using entangled photons without the fair-sampling assumption," *Nature*, vol. 497, no. 7448, p. 227, 2013.

[12] J. S. Bell, "Speakable and unspeakable in quantum mechanics," *Cambridge University*, 1987.

[13] J. Busck and H. Heiselberg, "Gated viewing and high-accuracy three-dimensional laser radar," *Applied optics*, vol. 43, no. 24, pp. 4705–4710, 2004.

DISTRIBUTION A: Distribution approved for public release. Distribution unlimited

[14] L. Dovrat, M. Bakstein, D. Istrati, A. Shaham, and H. S. Eisenberg, "Measurements of the dependence of the photon-number distribution on the number of modes in parametric down-conversion," *Optics express*, vol. 20, no. 3, pp. 2266–2276, 2012.

[15] J. Aasi, J. Abadie, B. Abbott, R. Abbott, T. Abbott, M. Abernathy, C. Adams, T. Adams, P. Addesso, R. Adhikari, *et al.*, "Enhanced sensitivity of the ligo gravitational wave detector by using squeezed states of light," *Nature Photonics*, vol. 7, no. 8, p. 613, 2013.

[16] Y. Israel, S. Rosen, and Y. Silberberg, "Supersensitive polarization microscopy using noon states of light," *Physical review letters*, vol. 112, no. 10, p. 103604, 2014.

[17] B. M. Escher, R. L. de Matos Filho, and L. Davidovich, "General framework for estimating the ultimate precision limit in noisy quantum-enhanced metrology," *Nature Physics*, vol. 7, no. 5, p. 406, 2011.

[18] L. Cohen, Y. Pilnyak, D. Istrati, A. Retzker, and H. S. Eisenberg, "Demonstration of a quantum error correction for enhanced sensitivity of photonic measurements," *Physical Review A*, vol. 94, no. 1, p. 012324, 2016.

[19] G. Khoury, H. S. Eisenberg, E. Fonseca, and D. Bouwmeester, "Nonlinear interferometry via fock-state projection," *Physical review letters*, vol. 96, no. 20, p. 203601, 2006.

[20] L. Cohen, E. S. Matekole, Y. Sher, D. Istrati, H. S. Eisenberg, and J. P. Dowling, "Thresholded quantum LIDAR: exploiting photon-number-resolving detection," *Physical Review Letters*, vol. 123, no. 20, p. 203601, 2019.

[21] J. H. Shapiro, "The quantum illumination story," *IEEE Aerospace and Electronic Systems Magazine*, vol. 35, no. 4, pp. 8–20, 2020.

[22] S. Barzanjeh, S. Pirandola, D. Vitali, and J. Fink, "Microwave quantum illumination using a digital receiver," *Science Advances*, vol. 6, no. 19, p. eabb0451, 2020.

[23] E. Lantz, "Comment on "thresholded quantum lidar: Exploiting photon-number-resolving detection"," *Physical Review Letters*, vol. 124, no. 19, p. 199302, 2020.

[24] M. Hayashi, *Quantum Information: An Introduction*. Springer, 2006.

[25] A. S. Holevo, *Quantum Systems, Channels, Information*. de Gruyter Studies in Mathematical Physics (Book 16), de Gruyter, November 2012.

[26] J. Watrous, *Theory of Quantum Information*. Cambridge University Press, Apr. 2018.

[27] M. M. Wilde, *Quantum information theory*. Cambridge University Press, second ed., 2017. arXiv:1106.1445.

[28] C. W. Helstrom, "Quantum detection and estimation theory," *Journal of Statistical Physics*, vol. 1, pp. 231–252, 1969.

DISTRIBUTION A: Distribution approved for public release. Distribution unlimited

[29] A. S. Holevo, "Statistical problems in quantum physics," in *Second Japan-USSR Symposium on Probability Theory*, vol. 330 of *Lecture Notes in Mathematics*, pp. 104–119, Springer Berlin / Heidelberg, 1973.

[30] C. W. Helstrom, *Quantum Detection and Estimation Theory*. New York: Academic, 1976.

[31] C. L. Degen, F. Reinhard, and P. Cappellaro, "Quantum sensing," *Reviews of Modern Physics*, vol. 89, p. 035002, July 2017.

[32] S. Lloyd, "Enhanced sensitivity of photodetection via quantum illumination," *Science*, vol. 321, no. 5895, pp. 1463–1465, 2008.

[33] Q. Zhuang, Z. Zhang, and J. H. Shapiro, "Entanglement-enhanced Neyman–Pearson target detection using quantum illumination," *Journal of the Optical Society of America B*, vol. 34, no. 8, pp. 1567–1572, 2017.

[34] C. Gerry and P. Knight, *Introductory Quantum Optics*. Cambridge University Press, November 2004.

[35] J. S. Ivan, K. K. Sabapathy, and R. Simon, "Operator-sum representation for bosonic Gaussian channels," *Physical Review A*, vol. 84, no. 4, p. 042311, 2011.

[36] C. W. Helstrom, "Detection theory and quantum mechanics," *Information and Control*, vol. 10, no. 3, pp. 254–291, 1967.

[37] R. S. Kennedy, "A near-optimum receiver for the binary coherent state quantum channel," *Quarterly Progress Report*, vol. 108, pp. 219–225, 1973.

[38] M. Takeoka and M. Sasaki, "Discrimination of the binary coherent signal: Gaussian-operation limit and simple non-gaussian near-optimal receivers," *Physical Review A*, vol. 78, no. 2, p. 022320, 2008.

[39] J. L. Habif, A. Jagannathan, S. Gartenstein, P. Amory, and S. Guha, "Quantum-limited discrimination of laser light and thermal light," *Optics Express*, vol. 29, no. 5, pp. 7418–7427, 2021.

[40] H. L. V. Trees, *Detection, Estimation, and Modulation Theory, Part I: Detection, Estimation, and Linear Modulation Theory*. John Wiley & Sons, Ltd., Sept. 2001.

[41] M. M. Wilde, M. Tomamichel, S. Lloyd, and M. Berta, "Gaussian hypothesis testing and quantum illumination," *Physical Review Letters*, vol. 119, no. 12, p. 120501, 2017.

[42] F. Dupuis, L. Kraemer, P. Faist, J. M. Renes, and R. Renner, "Generalized entropies," *XVIIth International Congress on Mathematical Physics*, pp. 134–153, 2013. arXiv:1211.3141.

DISTRIBUTION A: Distribution approved for public release. Distribution unlimited

[43] G. Lachs, "Theoretical aspects of mixtures of thermal and coherent radiation," *Physical Review*, vol. 138, no. 4B, p. B1012, 1965.

[44] L. Cohen, Y. Pilnyak, D. Istrati, N. M. Studer, J. P. Dowling, and H. S. Eisenberg, "Absolute calibration of single-photon and multiplexed photon-number-resolving detectors," *Physical Review A*, vol. 98, no. 1, p. 013811, 2018.

[45] M. Abadi, A. Agarwal, P. Barham, E. Brevdo, Z. Chen, C. Citro, G. S. Corrado, A. Davis, J. Dean, M. Devin, S. Ghemawat, I. Goodfellow, A. Harp, G. Irving, M. Isard, Y. Jia, R. Jozefowicz, L. Kaiser, M. Kudlur, J. Levenberg, D. Mané, R. Monga, S. Moore, D. Murray, C. Olah, M. Schuster, J. Shlens, B. Steiner, I. Sutskever, K. Talwar, P. Tucker, V. Vanhoucke, V. Vasudevan, F. Viégas, O. Vinyals, P. Warden, M. Wattenberg, M. Wicke, Y. Yu, and X. Zheng, "TensorFlow: Large-scale machine learning on heterogeneous systems," 2015. Software available from tensorflow.org.

[46] A. Serafini, *Quantum continuous variables: a primer of theoretical methods*. CRC press, 2017.

[47] K. Sharma, B. C. Sanders, and M. M. Wilde, "Optimal tests for continuous-variable quantum teleportation and photodetectors," *Physical Review Research*, vol. 4, no. 2, p. 023066, 2022.

[48] J. Clausen, T. Opatrnỳ, and D.-G. Welsch, "Conditional teleportation using optical squeezers and photon counting," *Physical Review A*, vol. 62, no. 4, p. 042308, 2000.

[49] Q. Zhuang, Z. Zhang, and J. H. Shapiro, "Quantum illumination for enhanced detection of rayleigh-fading targets," *Physical Review A*, vol. 96, no. 2, p. 020302, 2017.

DISTRIBUTION A: Distribution approved for public release. Distribution unlimited

Appendices (published with report):

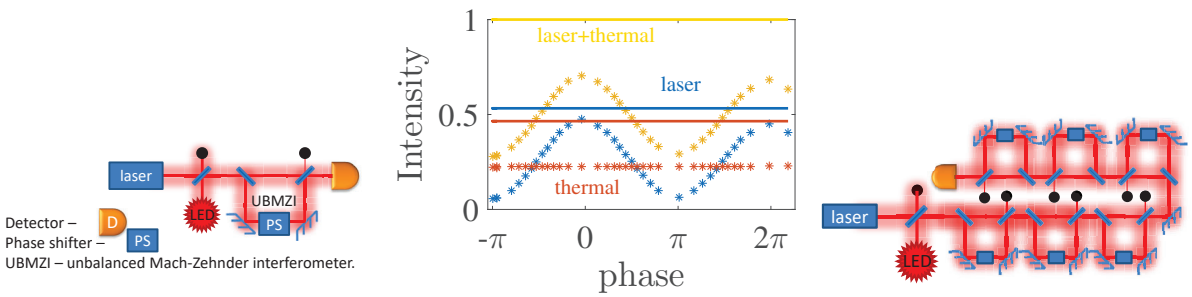

(a) (b) (c)

Figure 11: **(a)** The optical setup size is about one foot square, and the path difference is about 3 mm long. The phase was shifted by rotating a piece of window, increasing the optical path by a fraction of a wavelength. **(b)** Experimental results of laser only (blue), thermal light only (orange) and both (yellow). Solid lines represent the measured intensity without the unbalanced Mach-Zehnder interferometer and starred data points with it. For the phase of zero, the thermal intensity is cut to half while most of the laser intensity is preserved. **(c)** Schematic diagram of adding more interferometers. In this case, the thermal-light intensity is reduced by a factor of about 0.5^N where N is the number of interferometers. We note that the path difference cannot be the same in all interferometers.

Rejecting the thermal light with first order coherence:

The phenomenon of interference is governed by 'first order coherence.' If two meeting waves are coherent with each other, meaning the phase between them is locked, they interfere and the resulting amplitude of the interfered wave varies between the amplitude difference and sum of the original waves. If the phase between the two waves fluctuates rapidly, the interference is smoothed away to the averaged value.

One can interfere the same wave with itself at different times. Interference is observed when the two points are within the coherence time of the field. An unbalanced interferometer is one way of interfering the same light source in different times. Not all light sources have the same coherence time. In fact, lasers (usually used in LIDAR systems, e.g.) have very long coherence times compared to thermal sources (e.g. the solar radiation), where the ratio for short-pulse lasers can be as large as 10^6.

In order to demonstrate the advantage that can be utilized from different coherent times, we conduct an experiment in Prof. Hagai Eisenberg's lab at the Hebrew University of Jerusalem. A schematic diagram of the experiment setup is shown in Figure 3a. The laser and thermal light are spatially aligned on a beamsplitter, then directed into an unbalanced Mach-Zehnder interferometer, where one arm is 3 mm longer. The length difference, corresponding to 10 ps time difference (10^{-11} seconds), destroys the thermal-light interference but not the laser interference.

DISTRIBUTION A: Distribution approved for public release. Distribution unlimited

The results are presented in Figure 11b. Clearly when changing the phase, the laser intensity (blue stars) exhibits interference, while the thermal intensity (orange stars) exhibits no change. One would wish to work at the zero phase point, where the laser intensity keeps most of itself. At this point, the laser intensity keeps 89.3 percent while the thermal light keeps only 48.6 percent. The latter implies that 2.8 percent was lost due to the linear loss in the interferometer, and thus, 9.1 percent of the laser intensity is lost due to imperfect interference.

Now, we combine the laser and thermal light such that the SBR before the interferometer is 1.15. At the sweet spot after the interferometer, the SBR is 2.11, which introduces improvement by a factor of 1.84. Building a setup with N unbalanced interferometers (see Figure 11c), would improve the SBR exponentially by a factor of 1.84^N. We note that the SNR should show similar improvement.

Rejecting the thermal light with high order coherence:

Second-order correlation function, $g^{(2)}(\tau)$, has its origins in the Hanbury-Brown Twiss experiment, and is obtained by the intensity-intensity correlation: $g^{(2)}(\tau) = \langle I(t)I(t+\tau)\rangle / \langle I(t)\rangle^2$, where $\langle\cdot\rangle$ denotes average over time. Here, we try to exploit the different outputs of the correlation function of different states to get another method for finding the signal in LIDAR systems.

In the quantum analog of the correlation function, we replace the intensity by the number operator, $n = a^\dagger a$ ($a^\dagger$, a are the creation and annihilation operators) and perform normal order (putting the annihilation operators before the creation operators). Thus, the quantum second-order correlation function is

$$g^{(2)}(\tau) = \frac{\langle\psi|a^\dagger(t+\tau)a^\dagger(t)a(t+\tau)a(t)|\psi\rangle}{\langle\psi|a^\dagger(t)a(t)|\psi\rangle^2}\,, \tag{24}$$

where $\langle\psi|\cdot|\psi\rangle$ is the expectation value with respect to the state $|\psi\rangle$. The annihilation and creation operators may commute or partially commute at different times. This would reduce the value of the correlation function of the thermal light and reduce the difference from the correlation function of the laser light. Thus, we are mostly interested in the correlation function at zero:

$$g^{(2)}(0) = \frac{\langle\psi|n^2 - n|\psi\rangle}{\langle\psi|n|\psi\rangle^2} = \sum_{n=0}^{\infty} p(n)(n^2 - n)\,, \tag{25}$$

where $p(n)$ are the photon statistics of the state $|\psi\rangle$, and this formula was obtained by writing the state as a superposition of Fock (number) states. Now, we calculate the second-order correlation function of the mixed thermal-coherent light by substituting the statistics of Eq. (3):

$$g^{(2)}(0) = 1 + \left(\frac{\bar{n}_{\rm th}}{\bar{n}_{\rm th} + \bar{n}_{\rm p}}\right)^2. \tag{26}$$

It can be seen that in the limit of only laser or only thermal light, we get the well-known values of the correlation function.

DISTRIBUTION A: Distribution approved for public release. Distribution unlimited

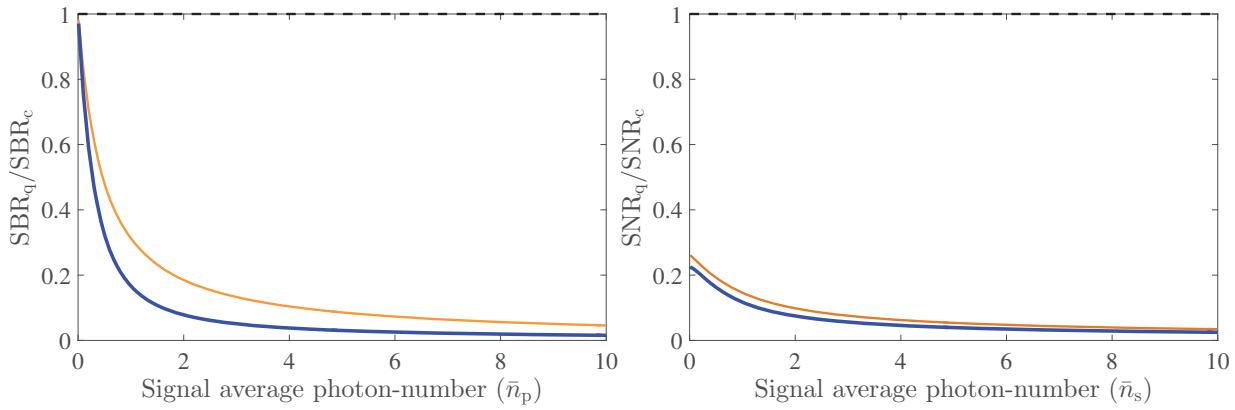

(a) (b)

Figure 12: The ratio of the quantum and classical SBR (a) and SNR (b) for fixed thermal average photon-number of one. $g^{(2)}$ results are plotted in orange and $g^{(3)}$ results are plotted in blue. The dashed black line at one represents the limit, above which the quantum scheme gets a better SBR/SNR.

To calculate the SBR of $g^{(2)}$, we divide the detection output of Eq. (26) with and without the laser photons:[1]

$$\mathrm{SBR_q} = 2\frac{(\bar{n}_{\mathrm{th}} + \bar{n}_{\mathrm{p}})^2}{(\bar{n}_{\mathrm{th}} + \bar{n}_{\mathrm{p}})^2 + (\bar{n}_{\mathrm{th}})^2}\,. \tag{27}$$

Our next step is to calculate the SNR. For that we use the error propagation formula to compute the error of the correlation function: $\Delta^2 g^{(2)}(0) = \frac{\partial^2 g^{(2)}(0)}{\partial \langle n\rangle^2}\Delta^2\langle n\rangle + \frac{\partial^2 g^{(2)}(0)}{\partial \langle n^2\rangle^2}\Delta^2\langle n^2\rangle$, where $\langle\cdot\rangle = \langle\psi|\cdot|\psi\rangle$ for shortcut, $\Delta^2\langle n^k\rangle = \langle n^{2k}\rangle - \langle n^k\rangle^2$, and $\langle n^k\rangle$ is the kth moment of the photon statistics. Substituting the latter relation and the derivatives, we get the noise to be: $\Delta^2 g^{(2)}(0) = \left(4\frac{\langle n^2\rangle^2}{\langle n\rangle^6} + \frac{1}{\langle n\rangle^4}\right)(\langle n^2\rangle - \langle n\rangle^2) + \frac{1}{\langle n\rangle^4}(\langle n^4\rangle - \langle n^2\rangle^2)$. Now we can write down the quantum SNR for $g^{(2)}(0)$:

$$\mathrm{SNR_q} = \frac{1 - \left(\frac{\bar{n}_{\mathrm{th}}}{\bar{n}_{\mathrm{th}}+\bar{n}_{\mathrm{p}}}\right)^2}{\sqrt{\Delta^2 g^{(2)}_{\mathrm{th}}(0) + \Delta^2 g^{(2)}_{\mathrm{mix}}(0)}}\,, \tag{28}$$

where $\Delta^2 g^{(2)}_{\mathrm{th}}(0)$, $\Delta^2 g^{(2)}_{\mathrm{mix}}(0)$ are the noise of the correlation function for the thermal light and mixed of thermal and coherent. We compare the SBR and SNR of $g^{(2)}$ to the classical ones by taking the ratio in Figure 12, where the results are plotted in orange. Unfortunately, the quantum SBR/SNR is always below the classical.

One might think this may be changed for higher-order correlation functions. Thus, we also check $g^{(3)}$ to reveal the tendency of the SBR/SNR while increasing the order of the correlation function. The procedure of calculating the quantum SBR and SNR of $g^{(2)}$ is

[1] we inverse the SBR to get something larger than 1, because we care only from the contrast.

DISTRIBUTION A: Distribution approved for public release. Distribution unlimited

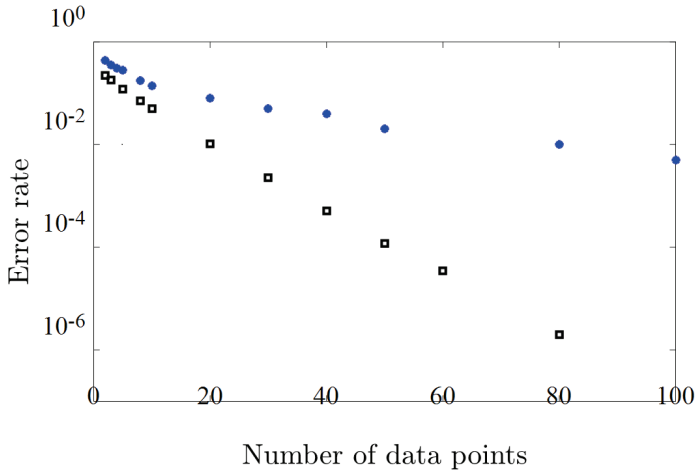

Figure 13: Comparison of symmetric error rates for machine learning and the optimal quantum detection.

repeated for $g^{(3)}$. Analytically, the quantum third-order correlation function is

$$g^{(3)}(0) = \frac{\langle\psi|a^{\dagger 3}a^3|\psi\rangle}{\langle\psi|a^\dagger a|\psi\rangle^3} = \frac{\langle\psi|n^3 - 3n^2 + 2n|\psi\rangle}{\langle\psi|n|\psi\rangle^3} = 1 + \frac{5\bar{n}_{\rm th}^3 + 3\bar{n}_{\rm th}^2\bar{n}_{\rm p}}{(\bar{n}_{\rm th} + \bar{n}_{\rm p})^3}\,, \tag{29}$$

where we first reorder the creation operators to write $g^{(3)}$ in terms of number operators, and then use the statistics of Eq. (3). Notice that for thermal light/ laser only this formula gives 6/1 which is the known result. From Eq. (29), one can calculate the quantum SBR/SNR of the third-order correlation function, as shown above. Here, we present the outcome visually in Figure 12 (blue lines). Not only that the SBR/SNR of $g^{(3)}$ is below the classical, but also it is below this of $g^{(2)}$, which suggests that taking higher orders only lowers the SBR/SNR.

Machine learning performance:

A side research direction of this project is to employ deep learning technique to discriminate the coherent and the mixture of the coherent and thermal light. We have used a two-dimensional convolution neural network with the help of TensorFlow library [45]. Our convolution neural network is very simple with just two convolution layers and three fully connected layers. The average errors of the machine learning code are presented by blue dots in Figure 13 and have shown a rapid decrease with the increment in the input data points. For more than 10 data points, the neural network has failed to follow the quantum limit scaling, presented by black empty boxes. The quantum limit has been obtained by simulations as described above but with multiple trails per testing. We believe the deviation from the quantum limit is a result of the high dimensionalilty, which cannot be reduced by the machine learning code, and thus cannot follow the quantum limit.

DISTRIBUTION A: Distribution approved for public release. Distribution unlimited